Journal of Power Sources 271 (2014) 87–96

Contents lists available at ScienceDirect

Journal of Power Sources

journal homepage: www.elsevier.com/locate/jpowsour

Influence of the electrolyte for the oxygen reduction reaction with Fe/N/C and Fe/N/CNT electrocatalysts

Carlota Domínguez [a], Francisco J. Pérez-Alonso [a, *], José L. Gómez de la Fuente [a], Shaeel A. Al-Thabaiti [b], Sulaiman N. Basahel [b], Abdurrahman O. Alyoubi [b], Abdulmohsen A. Alshehri [b], Miguel A. Peña [a], Sergio Rojas [a, *]

[a] Grupo de Energía y Química Sostenibles (EQS), Instituto de Catálisis y Petroleoquímica, CSIC, C/ Marie Curie, 2, L10, 28049 Madrid, Spain
[b] Chemistry Department, Faculty of Science, King Abdulaziz University, P.O. Box 80200, Jeddah 21589, Saudi Arabia

HIGHLIGHTS

- The performance of NPMCs for the ORR is affected by the pH.
- The nature of the electrolyte is not critical when ORR are measured at constant pH.
- Sulfates seem to adsorb more strongly on NPMCs than other anions.

GRAPHICAL ABSTRACT

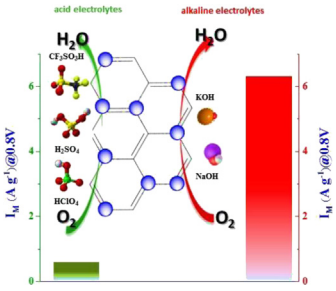

ARTICLE INFO

Article history:
Received 10 April 2014
Received in revised form
4 July 2014
Accepted 27 July 2014
Available online 2 August 2014

Keywords:
NPMC
Electrolyte
ORR
CNT
DRIFT
Fe

ABSTRACT

The behavior of Fe-based non-precious metal catalysts (NPMCs) in different electrolytes and the repercussion for the oxygen reduction reaction (ORR) has been studied. For this matter, a series of Fe-based NPMC electrocatalysts have been prepared from different carbon sources, carbon black and multiwalled carbon nanotubes. The catalysts have been subjected to chemical treatments in 0.5 M H_2SO_4 and thoroughly characterized. Their performance for the ORR in different electrolytes *e.g.* $HClO_4$, H_2SO_4, CF_3SO_3H, KOH and NaOH has been studied. Higher ORR rates have been recorded in the alkaline electrolytes as compared to the acid ones. Remarkably, the effect of the electrolyte is almost negligible when measured at a given pH value; *i.e.*, the ORR performance is not affected by the nature of the anion when measured in acid electrolytes or the cation when measured in alkaline electrolytes. On the other hand, the activity of NPMCs for the ORR decreases remarkably after treatment of the catalysts in 0.5 M H_2SO_4. This effect accounts to both the removal of active sites for the ORR during acid treatment and to the blockage of active sites due to the presence of adsorbed sulfates.

1. Introduction

Proton exchange membrane fuel cells (PEMFCs) have the potential to reduce today's society's dependence on fossil fuels and as a consequence they are expected to be widely implemented in the transportation sector and in portable devices. However, several economic and technological challenges are yet to be resolved. In

* Corresponding authors.
E-mail addresses: fperez@icp.csic.es (F.J. Pérez-Alonso), srojas@icp.csic.es (S. Rojas).

http://dx.doi.org/10.1016/j.jpowsour.2014.07.173
0378-7753/

particular, it is necessary to decrease the high loadings of Pt which are used in the state-of-the-art cathodes in order overcome the sluggish kinetics of the oxygen reduction reaction (ORR) resulting in very expensive PEMFCs. [1] In addition, features such as noble metal scarcity and Pt degradation in the cathode must be also considered for the designing of efficient ORR electrocatalysts. The design of alternative electrocatalysts with a significant reduction of Pt on their formulation [2] or even better, based upon non-expensive materials [3–6] is still a major challenge to implement real large-scale applications based on PEMFCs.

Non-precious metal catalysts (NPMCs) are strong candidates for replacing Pt in the cathode of PEMFCs. Although NPMCs with comparable ORR kinetic currents to the benchmark Pt/C have been reported recently [3,7–10], high-current-density performance and durability in acid media has to be improved significantly before NPMCs cathodes can replace Pt-based ones. In recent years numerous studies have been devoted to identify the nature of the active sites for the ORR within NPMCs [11–15], however, studies about the relationships between NPMCs and the reaction media, *i.e.*, the electrolyte are scarce. However, it is well-known that the nature of the electrolyte plays a key role in the performance of Pt-based catalysts for the ORR.

Seminal investigations with NPMCs for the ORR were inspired by nature and based on N_4-macrocycles of abundant elements such as cobalt and iron [16–20]. In this type of compounds, oxygen adsorption readily occurs at ambient temperature onto an iron center coordinated by four surrounding nitrogen functional groups [21]. However, these N_4-macrocycles coordinated to a metal center record no stable activity for the ORR in acidic media because the metal-N_x active site is destroyed by demetalation [17,18,22]. In this sense, it is well known that in order to obtain NMPCs with stable activity for the ORR in acid electrolytes a pyrolysis step above 600 °C in the presence of a nitrogen precursor, a transition metal precursor and a carbon matrix is necessary.

Graphene-coordinated FeN_4 and CoN_4 or FeN and CoN_2 moieties been proposed as the actual active sites in NPMCs [23–25]. Recently, Kramm et al. [12,13] studied the nature of the active sites for the ORR of Fe/N/C catalysts by using ^{57}Fe Mössbauer spectroscopy. They identified five different iron species and assigned the active site solely to an individual Fe(II) species within a FeN_4 arrangement with their ferrous ions both in a low or high spin. The same group reported that the N-surface groups which are part of this active site can bind anions such as sulfates from the electrolyte or HSO_3^- from Nafion membrane hence decreasing the measured turnover frequency for the ORR of the active sites [26]. These results clearly illustrate the importance that chemical changes on the catalyst surface may have for the ORR activity of NPMCs. It also shows that the understanding of the interrelations between the electrolyte and the NPMCs, in particular of the adsorption processes of the electrolyte onto NPMC surface, is paramount for the understanding of the catalytic performance for the ORR and consequently for the design of more active and robust NPMCs.

The effects of anion and cation adsorption for the ORR with Pt-based electrocatalysts are well documented [27–29]. In general, the presence of strongly adsorbed anions in the electrolytes such as H_2SO_4 or H_3PO_4 results in the appearance of high overpotentials for the ORR. This effect is not observed, however, when the ORR is measured in non-adsorbing electrolytes such as $HClO_4$, CF_3SO_3H or alkaline electrolytes. The observed decline of the ORR activity is related to strong anion adsorption of such electrolytes at the surface of Pt which impedes the adsorption of oxygen molecules onto the active sites. It is also well documented that the ORR performance of Pt/C is affected by the nature of the cation and decreasing in the order KOH > NaOH > LiOH [29]. This effect has been ascribed to non-covalent interaction between surface oxygenated species on Pt and the cation which results in the blocking of the active sites. However, studies for the effect of cation for the ORR with NPMCs are scarce. A recent study [30] shows that the cation influence for the ORR with perovskite catalysts ($LaMn_2O_{3+\delta}$) has both the same trend and order of magnitude than with Pt/C. However, the observed cation effect for the ORR is much smaller with a perovskite catalyst such as $Ba_{0.5}Sr_{0.5}Co_{0.8}Fe_{0.2}O_{3-\delta}$, and in fact it is only observed when comparing the catalytic performance in KOH and LiOH.

This work aims to investigate the effect of anion and cation binding onto Fe/N/C catalysts in different acid and basic electrolytes and the repercussions for the ORR. In addition, the effect of the strong adsorption of sulfates at the catalyst surface during the acid treatment used for the preparation of Fe/N/C and Fe/N/CNT has been also studied. Fe/N/C electrocatalysts have been synthesized by ball milling of a mixture of active carbon or carbon nanotubes, urea and Fe-phthalocyanine. Finally, the active sites have been created by pyrolysis at 800 °C under N_2 atmosphere. An aliquot of the obtained solid was treated in 0.5 M H_2SO_4 to removing the acid-soluble phases. The ORR of all catalysts before and after acid washing was evaluated by electrochemical means using an RDE (Rotating disk electrode) in the different electrolytes described above.

2. Experimental

2.1. Synthesis of Fe/N/C and Fe/N/CNT catalysts

The Fe/N/C catalysts studied in this work were prepared as follows. In a first step 5.5 g of the carbon matrix, either active carbon, (Norit GSX 94017-7) or multiwalled carbon nanotubes (CNTs) (Nanocyl NC 7000) and 0.2 g of the N precursor, 1,4,8,11-Tetraazacyclotetradecane (Aldrich 98%), were ballmilled, under room conditions, employing a planetary ballmill (PM100, Retsch), at 350 rpm during 4 h in a 50 mL WC vessel. The N/C composite obtained was mixed with 5.5 g of the carbon precursor (active carbon or CNTs) and 9.9 g of Urea (CH_4N_2O, PANREAC PRS) and ballmilled at 350 rpm during 4 h in a 50 mL WC vessel. In a following step the appropriate amount of iron phthalocyanine (Aldrich) to obtain a Fe concentration of 1.6 wt.% in the catalyst before pyrolysis, was added to 7.5 g of the N/C composite obtained after the two ball milling steps described above. This mixture was ballmilled again during 10 h at 350 rpm in a 50 mL WC vessel. The solid obtained was thermally treated (pyrolised) in a quartz tubular reactor at 800 °C for 1 h in an inert atmosphere of 25 mL min^{-1} of N_2. The resulting NPMCs were labeled as Fe/N/C or Fe/N/CNT where C and CNT denote whether the catalysts have been synthesized with active carbon or CNT, respectively. Aliquots of both catalysts were subjected to an acid-leaching, for this purpose samples were treated in 0.5 M H_2SO_4 (PANREAC QP) at 60 °C for 2 h to eliminate non-stable phases in acid electrolyte. The solid obtained was washed with distilled H_2O by centrifugation at 2500 rpm for 10 min until the pH of the recovered water was of ca. 6.5 and dried at 70 °C for 12 h. The NPMCs obtained acid leaching are labeled as L-Fe/N/C and L-Fe/N/CNT where L-prefix denote the acid treated catalysts.

2.2. Structural characterization

X-ray diffractograms were collected on a Seifert 3000 powder diffractometer operating with CuKα radiation (λ = 0.15418 nm) generated at 40 kV and 40 mA. Scans were recorded at 0.02°/s for 2θ values between 10° and 90°.

X-ray photoelectron spectra (XPS) of selected core-level elements were acquired with a VG Escalab 200R spectrometer fitted with an MgKα (hυ = 1253.6 eV) 120 W X-ray source. The energy

regions of the photoelectrons of interest were scanned until an acceptable signal-to-noise ratio was achieved. Intensities were estimated by calculating the integral of each peak, determined by subtraction of the Shirley-type background and fitting of the experimental curve to a combination of Lorentzian and Gaussian lines of variable proportions. Accurate binding energies (±0.2 eV) were determined by referencing to the C 1s peak at 284.6 eV.

Carbon, nitrogen, hydrogen and sulfur contents of the samples were measured with an elemental analyzer (LECO CHNS-932).

Infrared spectra (DRIFT) were obtained with a Jasco FTIR-6300A spectrometer equipped with an MCT detector. The spectra were recorded with a resolution of 4 cm^{-1} and an accumulation of 256 scans. Fe/N/C and L-Fe/N/C were finely ground and placed into a ceramic crucible in the DRIT chamber. In a first step, 25 mL min^{-1} of pure He was flowed through the chamber at 200 °C for 1 h to remove physisorbed H_2O. The temperature was set at 25 °C and DRIFT spectra were recorded for each sample and used as reference spectra. Then, Fe/N/C and L-Fe/N/C samples were subjected to a thermal treatment in He at 500 °C K for 1 h (heating rate 10 °C min^{-1}). Then, the temperature was decreased to 25 °C under He and DRIFT spectra for each sample were recorded.

Textural properties were evaluated by N_2 adsorption–desorption isotherms of the samples recorded at liquid N_2 temperature with a Micromeritics ASAP 2000 apparatus. Samples were degassed at 140 °C under vacuum for 24 h. Specific areas were calculated by applying the BET method within the relative pressure range $P/P^0 = 0.05–0.30$.

2.3. Electrochemical characterization

The electrochemical experiments were performed by using a computer controlled Autolab Pgstat 302N potentiostat/galvanostat.

A standard three-compartment glass cell and a rotating disk electrode (RDE) (Pine research Instruments) were used for all electrochemical experiments. The counter electrode was a graphite rod and the reference electrode was a Reversible Hydrogen Electrode (RHE). All potentials in this manuscript are referred to the RHE.

A glassy carbon electrode with a thin film of the electrocatalyst under study was used as the working electrode. For the thin film preparation of the Fe/N/C series the catalysts were dispersed ultrasonically in a mixture of Millipore Milli Q® water, and Nafion (5 wt.%) with a final ratio of 98 vol.% and 2 vol.%, respectively. For the Fe/N/CNT series the ink were prepared using a mixture of isopropanol, Millipore Milli Q® water and Nafion (5 wt.%) with a final ratio of 19.6 vol.%, 78.5 vol.% and 1.9 vol.%, respectively. The final concentration of the electrocatalyst in the suspension was 6 mg_{cat} mL^{-1}. A volume of 20 μL of the suspension was pipetted onto the previously polished glassy carbon tip (0.196 cm^2) of the RDE.

Previous to the electrochemical testing, the working electrode was electrochemically cleaned by potential cycling from 0 to 1.1 V for 50 cycles in Ar-saturated 0.1 M of the electrolyte used: CF_3SO_3H, H_2SO_4, $HClO_4$, KOH or NaOH, until stable voltammograms are obtained (Fig. S1). Cyclic voltammograms (CVs) were recorded between 0 and 1.0 V at 10 mV s^{-1} in Ar-saturated 0.1 M of the electrolyte used: CF_3SO_3H, H_2SO_4, $HClO_4$, KOH or NaOH.

The ORR polarization curves were collected by means of the RDE technique by recording a series of cyclic voltammograms between 0 V and 1 V at 10 mV s^{-1} and 1600 rpm in O_2-saturated in 0.1 M of the electrolyte used: CF_3SO_3H, H_2SO_4, $HClO_4$, KOH or NaOH. The Faradaic current density (j_F in mA cm^{-2}) was obtained by subtracting the current obtained during the anodic sweep scan in the O_2-saturated electrolyte from the capacitive current obtained in the potential sweep recorded in Ar-saturated O_2-free electrolyte under the same experimental conditions. The ORR kinetic current (i_k) was calculated by using the relationship between i_k and i_F as established by the Koutecky–Levich equation ($i_k = -i_F \cdot i_{lim}/(i_F - i_{lim})$) where i_K is the kinetic current defined as < 0 for reduction reactions and i_{lim} is the limiting current. Finally, the ORR mass activity is defined by $i_M = -i_K/m_{cat}$ where m_{cat} is the catalyst loading expressed in grams [31].

3. Results and discussion

3.1. Physicochemical characterization

Fig. 1 shows the diffractograms of Fe/N/C and L-Fe/N/C. Both diffractograms display a set of reflections characteristic of the Fe_3C phase along with a strong reflection of the (002) planes of graphite at $2\theta \approx 25°$. In addition, the diffractogram of Fe/N/C presents small diffractions peaks of Fe_3O_4 which are not observed in the diffractogram of L-Fe/N/C indicating that phase has been leached during the acid treatment in 0.5 M H_2SO_4. This observation is predictable due to the high solubility of Fe oxide and carbide phases in acid media. On the other hand, the diffraction peaks of the Fe_3C phase, although less intense, are still observed in the diffractogram of L-Fe/N/C suggesting that the Fe_3C is not completely removed during acid treatment even though this phase is also highly soluble in acid media such as 0.5 M H_2SO_4. In view of these results, it is plausible to assume that Fe_3C is encapsulated or strongly bound within the carbon matrix of L-Fe/N/C.

C, H, N and S contents (wt.%) have been determined by elemental analysis (see Table 1). The results obtained indicate that all of the N incorporated (around 4 wt.%) onto the carbon matrix after the pyrolysis process is stable after acid treatment confirming previous results [32]. As observed in Table 1, L-Fe/N/C contains a significant amount of S of 0.9 wt.%, much greater than S detected in Fe/N/C. The presence of S in the acid treated sample clearly indicates that sulfate anions remain adsorbed on the catalyst after the 0.5 M H_2SO_4 treatment.

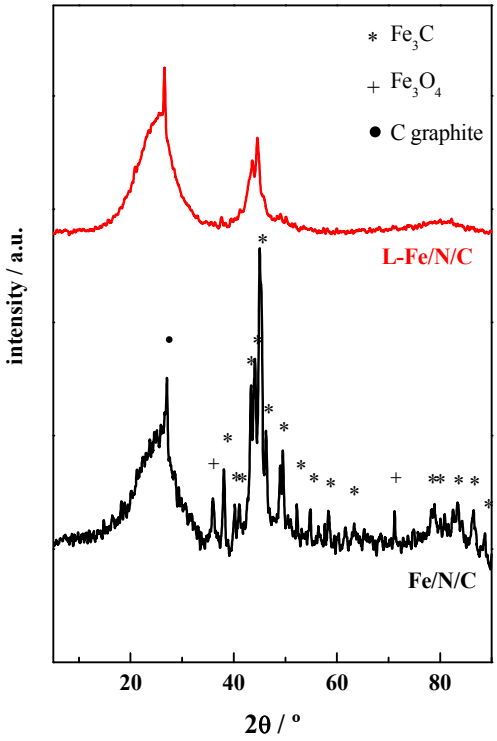

Fig. 1. X-ray diffraction patterns for L–Fe/N/C and Fe/N/C.

Table 1
C, H, N and S wt.% contents of the catalysts under study determined from elemental analysis. Specific surface areas determined form the BET method.

Catalyst	C wt.%	H wt.%	N wt.%	S wt.%	BET area/m^2g^{-1}
Fe/N/C	75.9	1.2	3.9	0.20	238.8
L–Fe/N/C	76.1	1.2	3.9	0.90	159.7
L–Fe/N/C-350	70.0	1.4	3.7	0.32	
Fe/N/CNT	84.8	0.5	2.5	0.01	160.6
L–Fe/N/CNT	87.2	0.5	2.6	0.28	145.1
L–Fe/N/CNT-350	86.2	0.5	2.6	0.16	

The Fe 2p, S 2p, C 1s, N 1s and O 1s core-level region spectra of Fe/N/C and L-Fe/N/C were recorded in order to estimate the relative surface abundance of these elements and to identify their nature, see Table 2. The N 1s and Fe 2p core-level spectra of Fe/N/C and L-Fe/N/C are shown in Fig. 2. The N 1s spectra comprise three components with peak maxima at 398.5, 400.1 and 401–401.5 eV. The peak at 398.5 eV corresponds to pyridinic forms of nitrogen (pyridinic-N), whereas the peak at 400.1 eV is assigned to pyrrolic nitrogen (pyrrolic-N) or/and to nitrogen in pyridones (pyridone-N). The N species at the highest binding energy of 401–401.5 eV are usually ascribed to quaternary nitrogen (graphitic-N) defined as relatively more positively charged nitrogen than pyridinic-N, and being part of a larger aromatic structure including protonated pyridinic-N and nitrogen atoms replacing carbon atoms in graphene structures [31,33,34].

As observed in Fig. 2 and in Table 2, the contribution of pyrrolic-N (and/or pyridone-N) to the total N-species increases at the expenses of the other N-species after the acid treatment in 0.5 M H_2SO_4. However, and in good agreement with the data recorded from elemental analyses (see Table 1), the total N_{at}/C_{at} surface atomic ratio remains stable after the acid treatment. On the other hand, the Fe_{at}/C_{at} surface atomic ratio decreases from 0.005 in Fe/N/C to 0.002 in L-Fe/N/C, confirming that a significant fraction of the Fe-containing phases have been removed during the acid treatment in 0.5 M H_2SO_4. Two distinct Fe species with peak maxima at 710.5 and 707.1 eV ascribed to Fe^{2+}/Fe^{3+} and Fe^0 species, respectively [35,36] can be observed in the Fe $2p_{3/2}$ core-level spectrum of Fe/N/C. This observation is in good agreement with the XRD analysis showing the coexistence of Fe_3O_4 and Fe_3C phases in Fe/N/C. The spectrum of L-Fe/N/C, however, contains a single less intense peak with maximum at around 710.5 eV indicative of the presence of Fe oxidized species. The decreasing of the intensity of the Fe 2p XPS indicates that a significant fraction of Fe species are removed during the acid treatment. This observation is also supported by the XRD data shown above which also show that previous to the acid treatment, Fe_3O_4 and Fe_3C crystal phases are present in Fe/N/C but only weak peaks of the latter species are observed in the diffractogram for L-Fe/N/C. The position of the Fe 2p core-level peak at ca. 710.5 eV for L-Fe/N/C along with the presence of a satellite line at ca. 715.5 eV is indicative of the presence of Fe^{2+} species. As a consequence, the Fe species remaining in L-Fe/N/C can be assigned to Fe/N*x* species, probably FeN_4 and/or FeN_{2+2}, which have been proposed as the active sites for the ORR reaction [37,38].

Table 2
N/C, S/C and Fe/C surface atomic ratios derived from XPS analysis of Fe/N/C and L–Fe/N/C samples.

Sample	Pyridinic-N	Pyrrolic-N	Quaternary-N	N/C	Fe/C	S/C
Fe/N/C	0.50	0.15	0.35	0.041	0.0050	–
L–Fe/N/C	0.43	0.25	0.32	0.042	0.0020	0.002
L–Fe/N/C-350	0.46	0.22	0.32	0.047	0.0025	–
Fe/N/CNT	0.55	0.28	0.12	0.026	0.0020	–
L–Fe/N/CNT	0.46	0.32	0.18	0.024	0.0010	0.001
L–Fe/N/CNT-350	0.49	0.39	0.09	0.021	0.0011	0.0007

The lack of XPS peaks for Fe-reduced species in the spectra of L-Fe/N/C indicates the removal of the fraction of the Fe_3C phase located at the surface of the catalyst during the acid treatment. However, since Fe_3C crystallites are clearly detected by XRD is reasonable to assume that a fraction of such phase is not soluble in acid media probably because it remains encapsulated within the carbon matrix and as a consequence it cannot be detected by a surface-sensitive technique such as XPS.

The S 2p core-level spectrum of L-Fe/N/C (Fig. 2c) shows a single component with peak maximum at 168.5 eV ascribed to sulfate (SO_4^{2-}) species. This observation is in line with the elemental analysis results which show that the amount of S-containing species increases after acid treatment with 0.5 M H_2SO_4. It has been recently reported that the ORR activity of NPMCs is severely affected by the presence of adsorbed sulfate species which bind to protonated pyridinic nitrogen which is proposed to be part of the active site for the ORR [26]. The importance of the electrolyte for the performance of NPMCs for the ORR, which is in fact widely recognized for Pt-based electrocatalysts [27–29], has not been thoroughly studied hitherto. In the next section the influence of the electrolyte (nature of anion and pH) for the performance of NPMCs for the ORR will be described.

3.2. Effect of the electrolyte for the ORR performance of Fe/N/C and L-Fe/N/C

Fig. 3 shows the cyclic voltammograms for Fe/N/C and L-Fe/N/C recorded at 10 mV s^{-1} in Ar saturated 0.1 M solutions of the electrolyte under study, namely $HClO_4$, H_2SO_4, CF_3SO_3H, KOH and NaOH. Fe/N/C and L-Fe/N/C record similar voltammograms in all acid electrolytes displaying a square wave profile typical of potential-independent capacitive responses [31] along with two peaks ascribed to the Fe^{2+}/Fe^{3+} redox couple. The anodic peak (Ep_a) appears at ca. 0.65 V in the voltammograms recorded with L-Fe/N/C regardless of the nature of the acid electrolyte. By contrary, the Ep_a varies with the nature of the acid electrolyte in the voltammograms for Fe/N/C. Thus, when measured in CF_3SO_3H or $HClO_4$ the Ep_a appears at ca. 0.79 V, shifting to less positive potential values of ca. 0.65 V when measured in H_2SO_4. It should be noted that this latter Ep_a value is the same as those recorded for the H_2SO_4-treated catalyst, L-Fe/N/C, in all of the acid electrolytes. These results suggest that the shifting towards less positive values of the Ep_a of the Fe^{2+}/Fe^{3+} pair in the voltammogram for Fe/N/C recorded in 0.1 M H_2SO_4 as compared to the other acid electrolytes, is due to the presence of sulfates on the surface of Fe/N/C resulting in the stabilization of the Fe^{3+} species, *i.e.*, facilitating the oxidation of Fe^{2+} and hence shifting the Ep_a to less positive values. This behavior suggests that sulfate anions adsorb more strongly on Fe/N/C than perchlorate or triflate anions.

On the other hand, both Fe/N/C and L-Fe/N/C exhibit similar cyclic voltammograms when recorded in the alkaline electrolytes. The voltammograms display a square wave profile, wider at the more negative potentials, typical of capacitive responses. Noticeably, the Fe^{2+}/Fe^{3+} redox pair is not observed in the voltammograms recorded in alkaline media (not even if the potential window is extended to more anodic and/or cathodic potentials).

Fig. 4 shows the ORR polarization curves of Fe/N/C and L-Fe/N/C after subtraction of their corresponding capacitive currents recorded in the electrolyte under study. Irrespective of the catalyst and the electrolyte, the polarization curves exhibit a mixed kinetic-diffusion controlled region and a diffusion limiting current region. Clearly, both Fe/N/C and L-Fe/N/C exhibit superior performances for the ORR in the alkaline electrolytes. Remarkably, the performance of both electrocatalysts varies significantly with the pH but it is not severely affected with the actual nature of the electrolyte; this is,

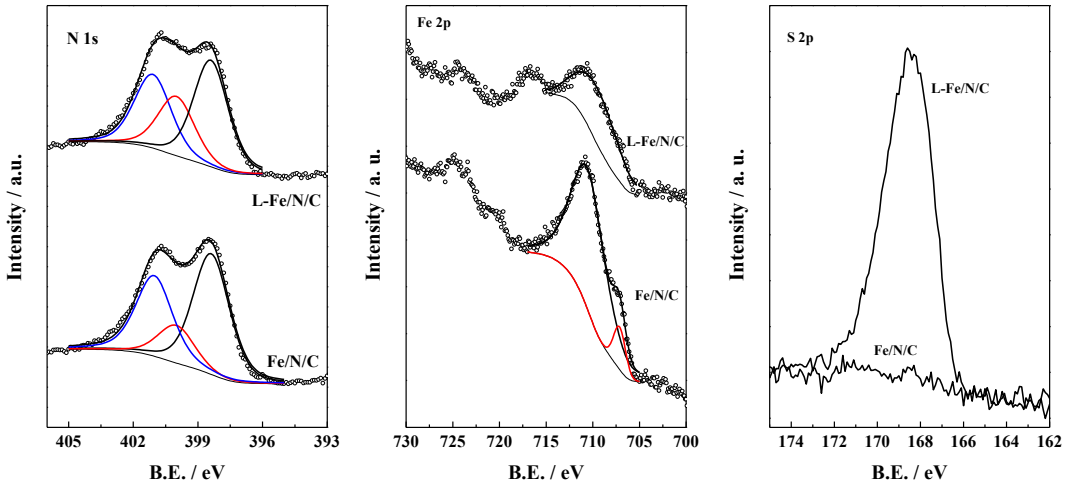

Fig. 2. XP spectra of the N 1s, Fe 2p and S 2p core-levels of Fe/N/C and L–Fe/N/C. The peaks for pyridinic-N, pyrrolic-N and quaternary-N in the N 1s core-level region spectrum are shown in black, red and blue, respectively. Fe^{2+}/Fe^{3+} and Fe^{0} components in the Fe 2p core-level region spectrum are shown in black and red, respectively. (For interpretation of the references to colour in this figure legend, the reader is referred to the web version of this article.)

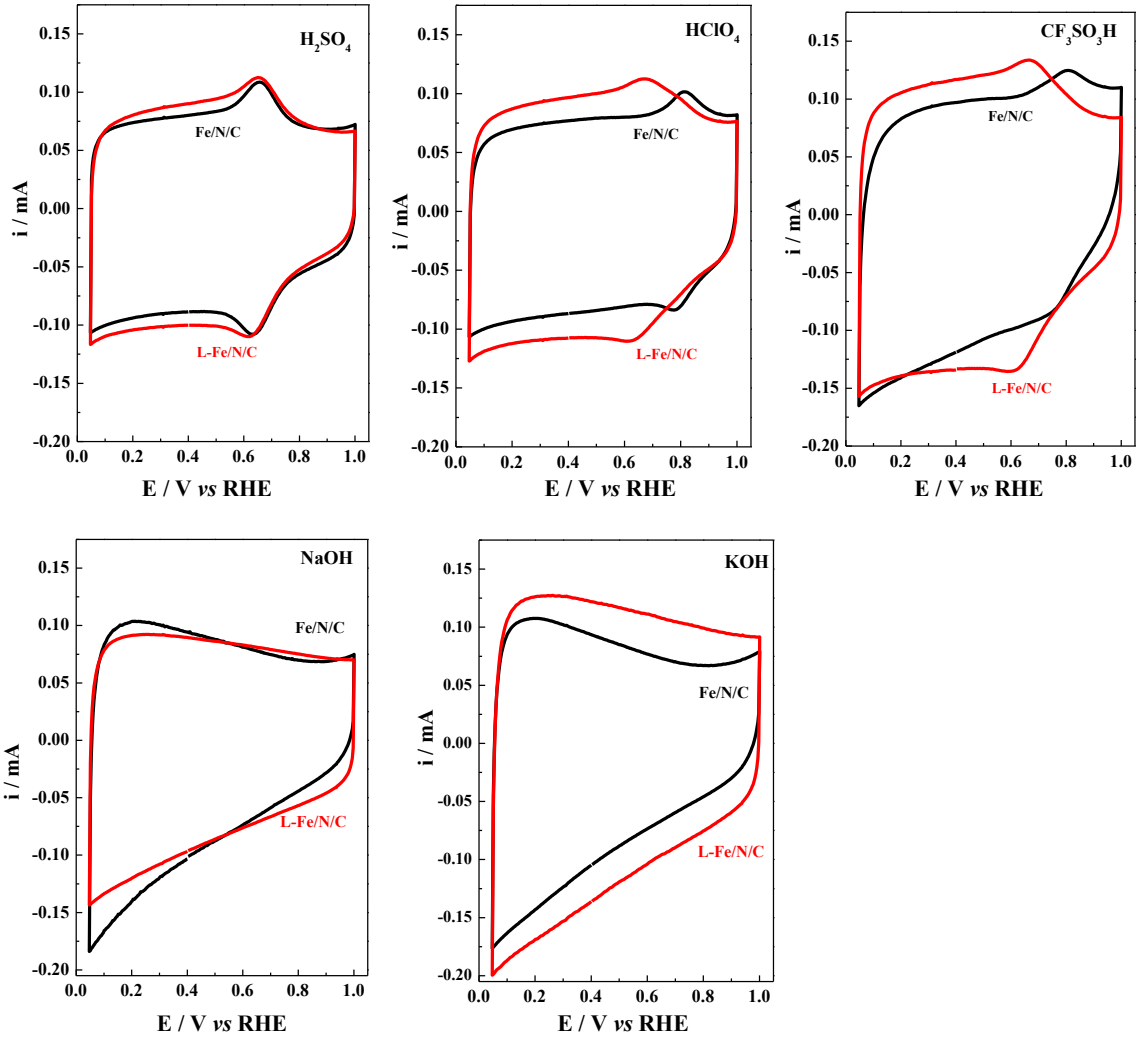

Fig. 3. Cyclic voltammograms for Fe/N/C (black lines) and L–Fe/N/C (red lines) recorded at 10 mV s^{-1} in 0.1 M of H_2SO_4, $HClO_4$, CF_3SO_3H, NaOH and KOH. Catalyst loading 0.6 mg cm^{-2}. (For interpretation of the references to colour in this figure legend, the reader is referred to the web version of this article.)

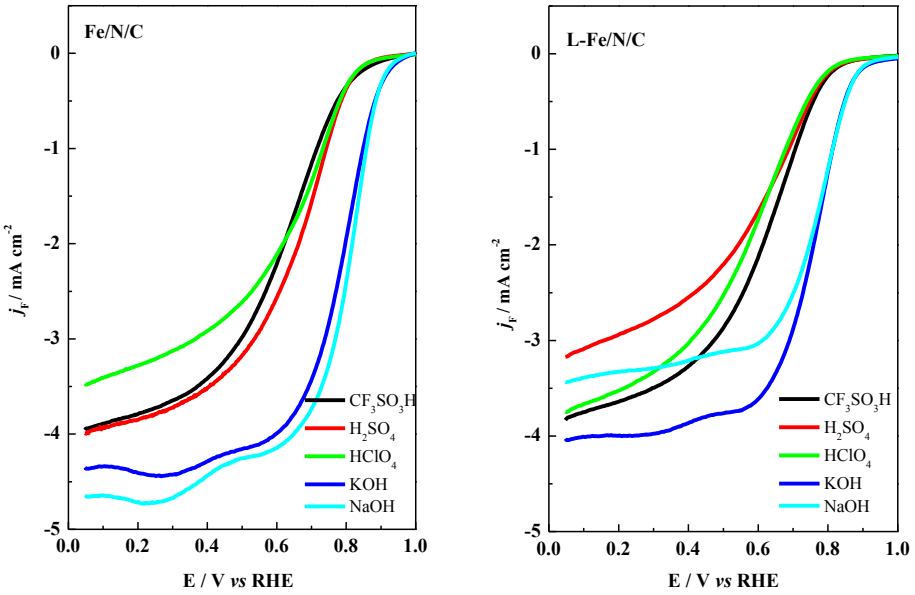

Fig. 4. Faradaic current densities (j_F) of Fe/N/C and L–Fe/N/C recorded during the positive going sweep in O_2 saturated 0.1 M electrolyte (as indicated in the legend) at 10 mVs^{-1}, 1600 rpm. Electrocatalyst loading 0.6 mg cm^{-2}.

similar performances are recorded in all alkaline electrolytes and in all acidic electrolytes. In addition, the current densities for Fe/N/C are higher than those recorded with L-Fe/N/C when measured in the same electrolytes.

Fig. 5 shows the mass transport corrected mass activities (i_M) of Fe/N/C and L-Fe/N/C in the kinetically controlled region which confirm the trends observed in the ORR polarization curves. The ORR performance varies with the pH and significantly higher ORR rates are recorded in alkaline electrolytes. However, the ORR kinetics is not severely affected by the nature of the anion (acid electrolytes) or the cations (alkaline electrolytes) and similar ORR rates have been recorded in all of the acid electrolytes and in all of the alkaline ones. As for the acid media, the ORR performance in CF_3SO_3H record a slightly different slope than that in H_2SO_4 and $HClO_4$ displaying higher i_M at low overpotentials and lower i_M at high overpotentials.

A previous study of Mukerjee et al. [39] reports that the higher activity of Fe/N/C catalysts for the ORR in alkaline media can be ascribed to the promotion of the direct molecular O_2 adsorption on the Fe^{2+} active site *vs* the outer-sphere mechanism (which follows the $2e^-$ pathway) which usually predominates for the ORR in alkaline media. This is because the OH^- species adsorbed at Fe^{2+} behave as a labile ligand hence being easily displaced by O_2. Ross et col. [40,41] studied the effect of pH in the ORR with noble metals and concluded that since the rate determining step (the transfer of one electron to $O_{2,ad}$ to $\cdot O_{2,ad}^-$) is a pH independent process, the

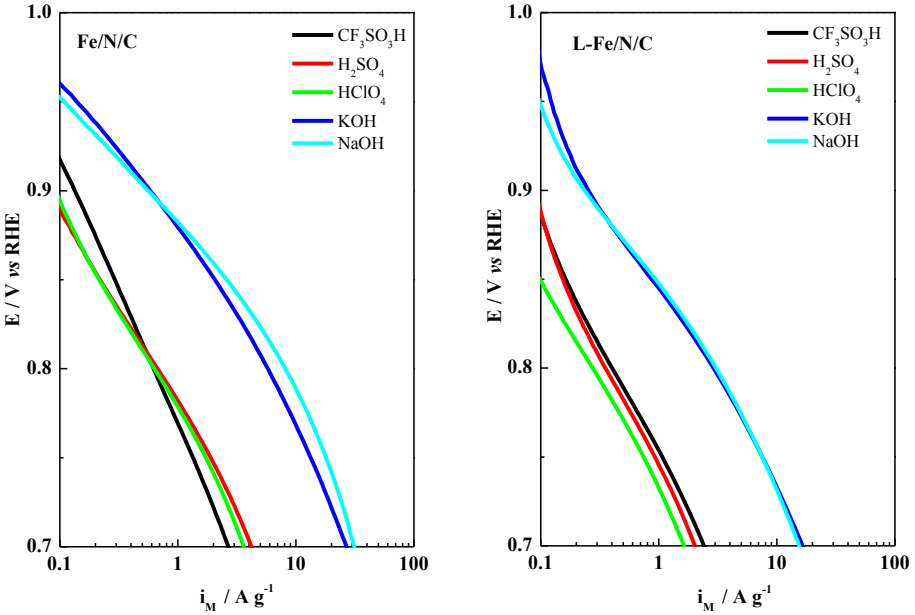

Fig. 5. Diffusion corrected mass activities (i_M) of Fe/N/C and L–Fe/N/C in O_2 saturated 0.1 M electrolyte at 10 mV s^{-1}, 1600 rpm. Sample loading 0.6 mg cm^{-2}.

reversible potential for the ORR should be pH independent as well. However, if the overall process is taken into account, by considering the involvement of H^+, then the overpotential becomes pH dependent decreasing with the increasing pH value.

Summarizing, our results clearly show that when measured at a given pH value, either acid or alkaline, the performance of Fe/N/C for the ORR is not severely influenced by the nature of electrolyte. The almost negligible effect of the cation or anion counterions for the ORR indicates that $CF_3SO_3^-$, ClO_4^- and SO_4^{2-} from the acid electrolytes or Na^+ and K^+ from the alkaline ones do not compete for the active sites with O_2 during the ORR or all cation or anion counterions compete in the same way. On the other hand, the observed shifting of the peaks for the Fe^{2+}/Fe^{3+} redox couple to more negative potentials in the cyclic voltammograms recorded in H_2SO_4 as compared to those recorded in $HClO_4$ or CF_3SO_3H see Fig. 3 indicate that sulfate anions adsorb more strongly than perchlorate or triflate ones on Fe/N/C. It has been suggested that a correlation between catalytic activity for the ORR and the potential of the M^{2+}/M^{3+} redox pair of metal N_4-macrocycles exists and that the more positive the Ep, the higher the catalytic activity for the ORR [42]. However, we have found no evidence for such a correlation between the Ep_a of the Fe^{2+}/Fe^{3+} and the performance for the ORR with the NPMCs reported in this manuscript. It should be noted that the actual nature of the NPMCs reported in this work, based upon the incorporation of Fe into N/C composites, is not the same than that of N_4-macrocyles reported in reference 42. In addition, a closer inspection of the blank voltammograms shown in Fig. 3 reveals that the amount of the Fe species responsible for the Fe^{2+}/Fe^{3+} pair is similar in both Fe/N/C and L-Fe/N/C. This observation is remarkable since the total amount of Fe in the latter sample is significantly lower than that in Fe/N/C (see Table 2) due to the dissolution of Fe species during the treatment in 0.5 M H_2SO_4. These conflicting observations suggest that the iron species responsible for the Fe^{2+}/Fe^{3+}pair (which appear to react with sulfates) might not actually be part of the active centers for the ORR.

3.3. Effect of sulfates for the ORR

As shown in Table 3, L-Fe/N/C exhibits between 37% and 47% lower i_M for the ORR at 0.8 V than Fe/N/C when measured in the acid electrolytes and between 50% and 60% lower activities when measured in alkaline media. One obvious reason for the lower ORR activity of L-Fe/N/C is the dissolution of a fraction of the Fe species during 0.5 M H_2SO_4 treatment. As shown in Table 2, the amount of Fe in L-Fe/N/C is around 60% lower than on Fe/N/C; however, it should be noted that not all of the Fe species within Fe/N/C are active for the ORR. A further cause for the observed decreasing ORR activity could be the blockage of the active sites by adsorbed sulfates. In fact, both XPS and chemical analyses indicate that S-containing species, more specifically sulfates as deduced from the peak at 168.5 eV characteristic of SO_4^{2-} species, see Fig. 2c, remain on L-Fe/N/C after the 0.5 M H_2SO_4 treatment. The presence of such sulfate species results in a severe decreasing of the BET area of Fe/N/C

Table 3
Mass activities at 0.8 V for Fe/N/C and L–Fe/N/C samples in O_2 saturated 0.1 M of different electrolytes studied at 10 mV s^{-1}, 1600 rpm. Sample loading 0.6 mg cm^{-2}.

Electrolyte	i_M at 0.8 V/A g^{-1}	
	Fe/N/C	L–Fe/N/C
CF_3SO_3H	0.60	0.38
H_2SO_4	0.63	0.34
$HClO_4$	0.59	0.31
KOH	5.50	2.70
NaOH	7.70	2.90

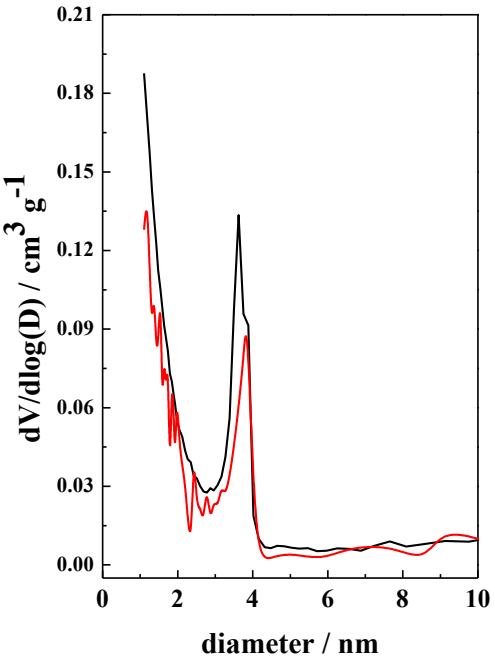

Fig. 6. Pore size distribution profiles for L–Fe/N/C (red line) and Fe/N/C (black line) samples. (For interpretation of the references to colour in this figure legend, the reader is referred to the web version of this article.)

from 239 m^2g^{-1} to 160 m^2g^{-1} recorded for L-Fe/N/C, as shown in Table 1. As shown in Fig. 6, the decreasing of the BET area is mainly due to the blockage of the micropores; it should be noted that the active sites for the ORR are proposed to be hosted in micropores [8,9].

In principle two hypotheses for the negative impact of adsorbed sulfates for the ORR can be proposed. On the one hand, sulfates would be adsorbed onto the micropores without forming chemical bonds and they simply hindering the access of O_2 into the active sites. On the other hand, actual chemical bonds between the sulfates and Fe or H bonded to N could be formed resulting in the poisoning of the active sites. The shifting of the E_{pc} and E_{pa} in the voltammograms for L-Fe/N/C (see Fig. 4) suggests that sulfates species could be interacting with Fe species. Moreover, the results shown in Table 2 show that the Fe/S surface atomic ratio is close to 1 for L-Fe/N/C suggesting a relationship exist between the amount of Fe on the catalysts and the amount of adsorbed sulfates. The question arises as to why L-Fe/N/C records visible activity for the ORR if all Fe sites are bonded to sulfates.

To elucidate the nature of the interaction between the adsorbed sulfates and the catalyst, DRIFT spectra for L-Fe/N/C were recorded at different temperatures. As shown in the Supplementary information section, and in good agreement with previous reports [26], it is possible to remove sulfates by subjecting L–Fe/N/C to thermal treatments under inert atmosphere. In order to remove sulfates, L–Fe/N/C was treated at 500 °C under N_2 within the DRIFT chamber and the DRIFT spectrum was collected at 20 °C. For the sake of comparison, DRIFT spectra were also recorded for Fe/N/C under the same protocol. The DRIFT spectra for L-Fe/N/C and Fe/N/C shown in Fig. 7 were obtained at 20 °C after subjecting the catalysts to a thermal treatment at 500 °C under N_2 (at 10° min^{-1}) during 30 min followed by subtraction of a reference spectrum recorded at 20 °C; as a consequence negative going bands indicate of the disappearance of adsorbed species. The spectrum for L-Fe/N/C depicts a broad

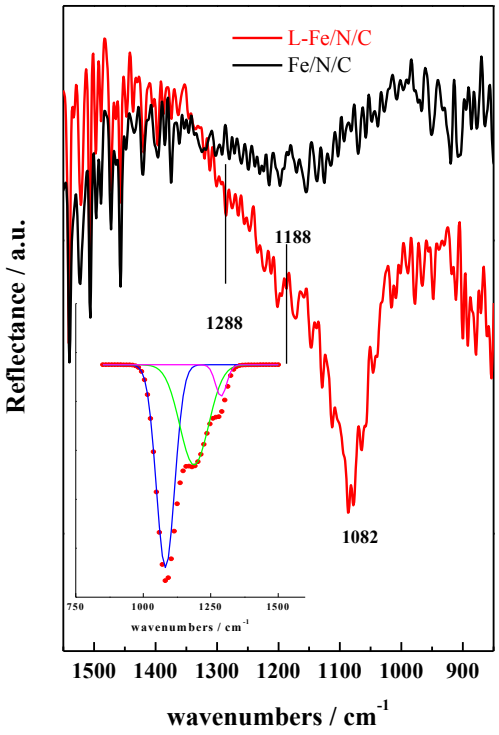

Fig. 7. DRIFT spectra recorded at room temperature of samples Fe/N/C and L–Fe/N/C after treatment in He at 500 °C during 1 h obtained after subtraction of spectra collected at 25 °C. The inset figure is the deconvolution of the band between 850 $cm^{-1}$and 1550 cm^{-1} of L–Fe/N/C.

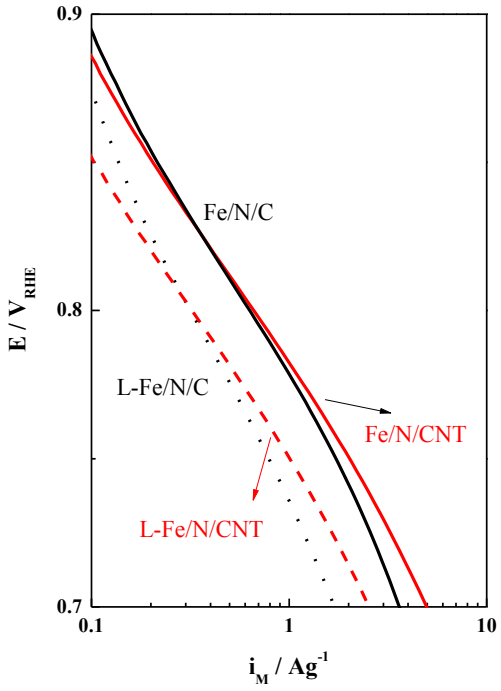

Fig. 8. Mass activities (i_M) for the ORR with Fe/N/C (black line), L–Fe/N/C (black dotted line), Fe/N/CNT (red line) and L–Fe/N/CNT (red dotted line) in O_2 saturated 0.1 M $HClO_4$ at 10 mV s^{-1}, 1600 rpm. Sample loading 0.6 mg cm^{-2}. (For interpretation of the references to colour in this figure legend, the reader is referred to the web version of this article.)

negative-going asymmetric band with maximum at around 1082 cm^{-1} tailing to higher frequencies showing two shoulders at ca. 1188 and 1288 cm^{-1}; the position of the peak maxima and the relative intensity of the less intense peaks is clearly observed after baseline correction and spectral fitting with Gaussian curves as shown in the inset to Fig. 7. This broad band, assigned to adsorbed sulfates is not observed in the spectrum of Fe/N/C. The results shown in Table 2 show that the Fe/S surface atomic ratio Fe/N/C is close to 1 for L–Fe/N/CNT suggesting that sulfates might be interacting with Fe species. In fact, the FTIR spectra for $FeSO_4 \cdot 7H_2O$ exhibit a very intense band at 1083 cm^{-1}. However, the FTIR spectra for $(NH_4)_2SO_4$ records a very strong band at 1078 cm^{-1}, so the assignment of the band at 1082 cm^{-1} is not straightforward. Besides, it should be taken into account that the spectra shown in Fig. 7 are for sulfates adsorbed on a solid, so FTIR spectra showing different bands, or more likely, shifting in the frequency of the characteristic bands can be obtained. The relationship between the symmetry of sulfate species forming chemical bonds with species located at the surface of a solid and their infrared spectra has been studied previously [43,44]. The presence of a single broad peak at around 1080 cm^{-1} is indicative of the presence of outer-sphere complexes of sulfates which retain their water of hydration and form no surface chemical bonds displaying a spectrum similar to aqueous sulfate. On the other hand, a metal-sulfate chemical bond, either monodentate or bidentate, results in a lower symmetry of sulfate characterized by an active band at 975 cm^{-1} and three or two different bands above 1000 cm^{--1} depending on whether the complex is bidentate or monodentate, respectively. The most intense band in the DRIFT spectra shown in Fig. 7 at 1082 cm^{-1} indicates the presence of non-bonded sulfates. Moreover, the lack of the band at 975 cm^{-1} suggests that sulfates are not bonded to metal centers. On the other hand, the bands at 1188 and 1288 cm^{-1} are indicative of the presence of metal-sulfate bonds.

The presence of sulfates adsorbed on Fe/N/C catalysts after H_2SO_4 treatment and their negative effect for the ORR has been observed by Herranz et al. [26] They proposed that sulfates react with –NH groups vicinal to FeN_x sites, rather than with Fe, resulting in a decreasing of the turnover of frequency (TOF) for the ORR. This proposal explains the lack of bands at 975 cm^{-1} in our DRIFT spectra which are indicative of sulfate bonding to Fe and justify the lower activity of L-Fe/N/C for the ORR. However, the implication of the presence of non-bonded sulfates for the ORR, if any, is not clear. In order to get a better understanding of the interaction between sulfates and the actives sites for the ORR we have prepared similar NPMCs based upon multiwalled carbon nanotubes so that the effect of microporosity can be neglected.

3.4. Synthesis and ORR performance of Fe/N/CNT and L-N/CNT

Fe/N/CNT and L-Fe/N/CNT have been synthesized by using a non-porous carbonaceous support, multiwalled carbon nanotubes (CNT), and following the same protocols as described above for the synthesis of Fe/N/C and L-Fe/N/C. In line with the results obtained for Fe/N/C series, Fe oxides and Fe_3C phases are observed in Fe/N/CNT and L-Fe/N/CNT (X-ray diffractograms are shown in Fig. S2). Also, three different N species (pyridinic, pyrrolic and quaternary) are observed by XPS (see Fig. S3). The main difference between both series of catalysts is that the amounts of N and Fe in Fe/N/CNT are ca. 33% lower than those in Fe/N/C (see Tables 1 and 2 for further details). Similar to Fe/N/C, acid treatment in 0.5 M H_2SO_4 of Fe/N/CNT leads to a significant decreasing of the Fe content by dissolution of the soluble Fe species along with the appearance of adsorbed sulfates (see XPS in Fig. S3). As shown in Table 1, the amount of

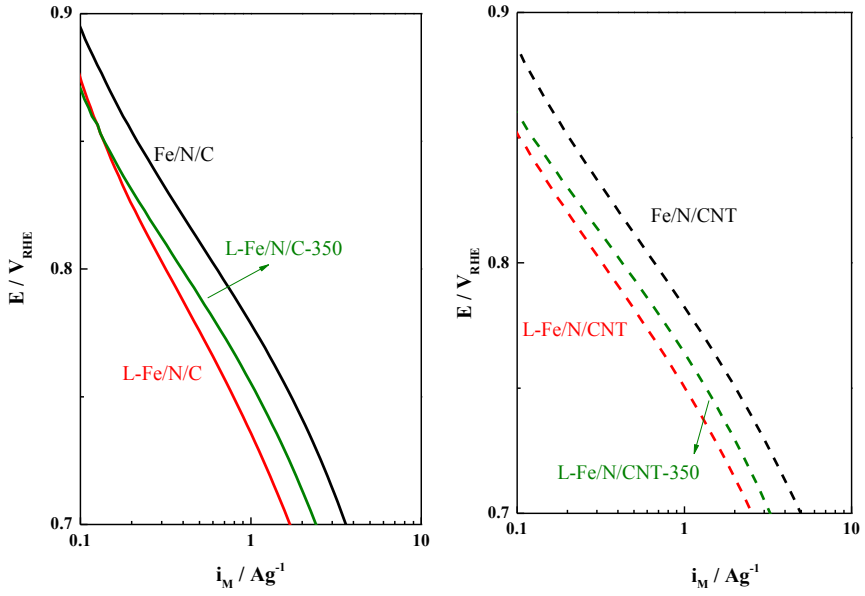

Fig. 9. Mass activities (i_M) of Fe/N/C, L–Fe/N/C and L–Fe/N/C-350 (left panel) and Fe/N/CNT, L–Fe/N/CNT and L–Fe/N/CNT-350 (right panel) in O_2 saturated 0.1 M $HClO_4$ at 10 mV s^{-1}, 1600 rpm. Sample loading 0.6 mg cm^{-2}.

S remaining on L-Fe/N/CNT is significantly lower than that recorded for L-Fe/N/C. However, and in good agreement with the results described above for L-Fe/N/C, the Fe/S surface atomic ratio for Fe/N/CNT is close to 1 (see Table 2), suggesting that a relation between the amount of Fe and the amount of adsorbed sulfates also exists when CNTs are used as the carbon source.

The cyclic voltammograms for Fe/N/CNT and L-Fe/CNT follow the same trend as those observed for Fe/N/C, *i.e.*, the presence of adsorbed sulfates leads to a shifting of the redox peaks to lower potentials (see Fig. S5). Finally, the BET area value of the CNT-based catalysts is smaller than that of the C-ones, but it is invariant after H_2SO_4 treatment.

As shown in Fig. 8, and despite of the lower amount of Fe and N, Fe/N/CNT records a similar mass activity (i_M) for the ORR than Fe/N/C. Moreover, the loss of ORR activity recorded with L–Fe/N/CNT is similar to that observed for L–Fe/N/C.

As stated above, the loss of ORR performance is due to both the removal of acid soluble Fe species and the presence of sulfates onto the actives sites. In order to remove adsorbed sulfates, L–Fe/N/C and L–Fe/N/CNT were subjected to thermal treatments at 350 °C under N_2 for 1 h and the solid obtained were labeled as L–Fe/N/C-350 and L-Fe/N/CNT-350, respectively. This temperature was set after the thermal gravimetric analysis shown in Fig. S4. Clearly, the amount of sulfates decreases after the thermal treatment, and in fact, sulfates are not detected in the surface of neither L–Fe/N/C-350 nor L–Fe/N/CNT-350 by XPS (see Table 2). As shown in Fig. 9, the ORR mass activity of L–Fe/N/C-350 and L–Fe/N/CNT-350 increases after the thermal treatment but the complete recovery of the ORR performance is not achieved. This is a clear indication that the loss of activity is also due to the dissolution of a fraction of the Fe species during treatment in 0.5 M H_2SO_4. Remarkably, the recovered activity is very similar for both catalysts.

The results shown in this section clearly show adsorbed sulfates on NPMCs have a negative impact for the ORR. Moreover, the nature of the interaction between adsorbed sulfates and the catalyst is not affected by the nature of the carbon source used for the preparation of the catalyst. As a consequence, similar ORR activity losses are recorded with NMPCs prepared with active carbon or with carbon nanotubes.

4. Conclusions

The performance of Fe/N/C for the ORR is severely affected by the pH of the electrolyte. Higher ORR activities are recorded in alkaline electrolytes as compared to acidic ones. However, the effect of the counterion, *i.e.*, of the anion or cations when measured under acidic or alkaline electrolytes, respectively, is almost negligible. On the other hand, if during the synthesis of Fe/N/C or Fe/N/CNT acid treatments are used, anions such as sulfates will become adsorbed onto the active sites resulting in a severe decrease of the ORR performance. The observed negative impact of the presence of sulfates for the ORR for both Fe/N/C and Fe/N/CNT indicates that sulfates remain bonded to the active sites rather than simply blocking the access of O_2 into the active sites.

Acknowledgments

This project was funded by the Deanship of Scientific Research (DSR), King Abdulaziz University, Jeddah, under grant number (D-006-432). The authors, therefore, acknowledge with thanks DSR technical and financial support. Economic support from projects ENE2010-15381 from the Spanish Ministry of Science and Innovation and Project 201080E116 from the CSIC is also acknowledged.

Appendix A. Supplementary data

Supplementary data related to this article can be found at http://dx.doi.org/10.1016/j.jpowsour.2014.07.173.

References

[1] H.A. Gasteiger, S.S. Kocha, B. Sompalli, F.T. Wagner, Appl. Catal. B 56 (2005) 9–35.
[2] I.E.L. Stephens, A.S. Bondarenko, U. Grønbjerg, J. Rossmeisl, I. Chorkendorff, Energy Environ. Sci. 5 (2012) 6744–6762.
[3] F. Jaouen, E. Proietti, M. Lefèvre, R. Chenitz, J.P. Dodelet, G. Wu, H.T. Chung, C.M. Johnston, P. Zelenay, Energy Environ. Sci. 4 (2011) 114–130.
[4] Y. Feng, T. He, N. Alonso-Vante, Chem. Mater. 20 (2008) 26–28.
[5] E. Vayner, R.A. Sidik, A.B. Anderson, B.N. Popov, J. Phys. Chem. C 111 (2007) 10508–10513.

[6] H. Zhong, H. Zhang, G. Liu, Y. Liang, J. Hu, B. Yi, Electrochem. Commun. 8 (2006) 707–712.
[7] G. Wu, K.L. More, C.M. Johnston, P. Zelenay, Science 332 (2011) 443–447.
[8] M. Lefèvre, E. Proietti, F. Jaouen, J.P. Dodelet, Science 324 (2009) 71–74.
[9] E. Proietti, F. Jaouen, M. Lefèvre, N. Larouche, J. Tian, J. Herranz, J.P. Dodelet, Nat. Commun. 2 (2011).
[10] G. Wu, P. Zelenay, Acc. Chem. Res. 46 (2013) 1878–1889.
[11] M. Ferrandon, A.J. Kropf, D.J. Myers, K. Artyushkova, U. Kramm, P. Bogdanoff, G. Wu, C.M. Johnston, P. Zelenay, J. Phys. Chem. C 116 (2012) 16001–16013.
[12] U.I. Kramm, J. Herranz, N. Larouche, T.M. Arruda, M. Lefèvre, F. Jaouen, P. Bogdanoff, S. Fiechter, I. Abs-Wurmbach, S. Mukerjee, J.P. Dodelet, Phys. Chem. Chem. Phys. 14 (2012) 11673–11688.
[13] U.I. Kramm, M. Lefèvre, N. Larouche, D. Schmeisser, J.-P. Dodelet, J. Am. Chem. Soc. 136 (2013) 978–985.
[14] S. Yasuda, L. Yu, J. Kim, K. Murakoshi, Chem. Commun. 49 (2013) 9627–9629.
[15] C. Domínguez, F.J. Pérez-Alonso, M. Abdel Salam, J.L. Gómez de la Fuente, S.A. Al-Thabaiti, S.N. Basahel, M.A. Peña, J.L.G. Fierro, S. Rojas, Int. J. Hydrogen Energy 39 (2014) 5309–5318.
[16] R. Jasinski, Nature 201 (1964) 1212–1213.
[17] S. Baranton, C. Coutanceau, C. Roux, F. Hahn, J.M. Léger, J. Electroanal. Chem. 577 (2005) 223–234.
[18] A.A. Tanaka, C. Fierro, D. Scherson, E.B. Yeager, J. Phys. Chem. 91 (1987) 3799–3807.
[19] A. van der Putten, A. Elzing, W. Visscher, E. Barendrecht, J. Electroanal. Chem. Interfacial Electrochem. 221 (1987) 95–104.
[20] J.H. Zagal, Coord. Chem. Rev. 119 (1992) 89–136.
[21] A.J.B. Alberts, J. Lewis, M. Raff, K. Roberts, P. Walter, Molecular Biology of the Cell, New York, 2002.
[22] H. Meier, U. Tschirwitz, E. Zimmerhackl, W. Albrecht, G. Zeitler, J. Phys. Chem. 81 (1977) 712–718.
[23] A.L. Bouwkamp-Wijnoltz, W. Visscher, J.A.R. Van Veen, E. Boellaard, A.M. Van der Kraan, S.C. Tang, J. Phys. Chem. B 106 (2002) 12993–13001.
[24] M. Lefevre, J.P. Dodelet, P. Bertrand, J. Phys. Chem. B 109 (2005) 16718–16724.
[25] U.I. Koslowski, I. Abs-Wurmbach, S. Fiechter, P. Bogdanoff, J. Phys. Chem. C 112 (2008) 15356–15366.
[26] J. Herranz, F. Jaouen, M. Lefèvre, U.I. Kramm, E. Proietti, J.P. Dodelet, P. Bogdanoff, S. Fiechter, I. Abs-Wurmbach, P. Bertrand, T.M. Arruda, S. Mukerjee, J. Phys. Chem. C 115 (2011) 16087–16097.
[27] N. Markovic, H. Gasteiger, P.N. Ross, J. Electrochem. Soc. 144 (1997) 1591–1597.
[28] J.S. Spendelow, A. Wieckowski, Phys. Chem. Chem. Phys. 9 (2007) 2654–2675.
[29] D. Strmcnik, K. Kodama, D. van der Vliet, J. Greeley, V.R. Stamenkovic, N.M. Marković, Nat. Chem. 1 (2009) 466–472.
[30] J. Suntivich, E.E. Perry, H.A. Gasteiger, Y. Shao-Horn, Electrocatalysis 4 (2013) 49–55.
[31] F. Jaouen, J. Herranz, M. Lefèvre, J.P. Dodelet, U.I. Kramm, I. Herrmann, P. Bogdanoff, J. Maruyama, T. Nagaoka, A. Garsuch, J.R. Dahn, T. Olson, S. Pylypenko, P. Atanassov, E.A. Ustinov, ACS Appl. Mater. Interfaces 1 (2009) 1623–1639.
[32] F.J. Pérez-Alonso, M.A. Salam, T. Herranz, J.L. Gómez De La Fuente, S.A. Al-Thabaiti, S.N. Basahel, M.A. Peña, J.L.G. Fierro, S. Rojas, J. Power Sources 240 (2013) 494–502.
[33] J.R. Pels, F. Kapteijn, J.A. Moulijn, Q. Zhu, K.M. Thomas, Carbon 33 (1995) 1641–1653.
[34] H.S. Oh, J.G. Oh, W.H. Lee, H.J. Kim, H. Kim, Int. J. Hydrogen Energy 36 (2011) 8181–8186.
[35] F. Bonnet, F. Ropital, P. Lecour, D. Espinat, Y. Huiban, L. Gengembre, Y. Berthier, P. Marcus, Surf. Interface Anal 34 (2002) 418–422.
[36] C.S. Kuivila, J.B. Butt, P.C. Stair, Appl. Surf. Sci. 32 (1988) 99–121.
[37] H.R. Byon, J. Suntivich, E.J. Crumlin, Y. Shao-Horn, Phys. Chem. Chem. Phys. 13 (2011) 21437–21445.
[38] J. Yang, D.J. Liu, N.N. Kariuki, L.X. Chen, Chem. Commun. (2008) 329–331.
[39] N. Ramaswamy, S. Mukerjee, Adv.Phys. Chem. 2012 (2012).
[40] B.B. Blizanac, P.N. Ross, N.M. Markovic, Electrochimica Acta 52 (2007) 2264–2271.
[41] P.N. Ross, Why Is Pt So Unique. A Chemical Physics Approach, https://www1.eere.energy.gov/hydrogenandfuelcells/pdfs/phil_ross.pdf.
[42] J. Masa, K. Ozoemena, W. Schuhmann, J.H. Zagal, J. Porphyrins Phthalocyanines 16 (2012) 761–784.
[43] D. Peak, R.G. Ford, D.L. Sparks, J.Colloid Interface Sci. 218 (1999) 289–299.
[44] K. Nakamoto, Infrared and Raman Spectra of Inorganic and Coordination Compounds, New York, 1986.